Gas phase hyper-Rayleigh scattering measurements

David P. Shelton
Department of Physics and Astronomy, University of Nevada, Las Vegas, Nevada 89154-4002, USA

(Received 1 June 2012; accepted 9 July 2012; published online 30 July 2012)

Measurements of hyper-Rayleigh scattering intensities and polarization ratios are presented for nine small molecules in the gas phase [CH_4, CF_4, CCl_4, N_2O, NH_3, D_2O, SO_2, CF_2Cl_2, and $(CH_3)_2CO$]. In four cases [CH_4, CF_4, CCl_4, and N_2O] all molecular hyperpolarizability tensor components can be determined from the measurements. The results of this experiment are compared with the results of previous *ab initio* calculations, finding discrepancies up to 60%. Including vibrational contributions decreases the discrepancies for CH_4 and CF_4 and increases them for CCl_4, D_2O, and NH_3. © *2012 American Institute of Physics*. [http://dx.doi.org/10.1063/1.4738897]

I. INTRODUCTION

Molecular first hyperpolarizabilities β are usually measured in the condensed phase, whereas *ab initio* calculations of β are usually for isolated molecules. Although calculation methods for molecules in the condensed phase are currently being developed, quantitatively accurate predictive calculations of the nonlinear optical properties of materials are difficult since they require careful treatment of many different physical effects.[1] The calculated results are sensitive to basis set and correlation treatment, molecular geometry and vibration, and interactions with the solvent. Adequate *ab initio* calculation methods for gas phase molecular hyperpolarizabilities, tested and calibrated against accurate experimental measurements of gas phase molecular hyperpolarizabilities, are the first step in developing adequate calculation methods for condensed phase nonlinear optical properties.[2]

There is limited experimental data on the gas phase hyperpolarizabilities of molecules to serve as benchmarks for assessing the theoretical calculations. Almost all the existing data are from electric-field-induced second harmonic generation (ESHG) measurements of a single combination of tensor components, $\beta_{||} = (1/5)\sum_i \{\beta_{zii} + \beta_{izi} + \beta_{iiz}\}$, the vector component of β in the direction of the molecular dipole moment.[3] Hyper-Rayleigh scattering (HRS) measurements have the potential to provide up to six independent pieces of information about the β tensor, and in the most favourable cases could determine all components of the β tensor.[4–7] This work presents gas phase HRS measurements which attempt to determine β tensor components for several small molecules of high symmetry. These experimental results are then compared with corresponding results from existing *ab initio* calculations for these molecules.

II. HRS POLARIZATION DEPENDENCE

The usual 90° scattering configurations with incident and scattered light linearly polarized either perpendicular or parallel to the horizontal scattering plane are denoted VV, HV, VH, and HH, where V denotes vertical polarization, H denotes horizontal polarization, and the first and second letters refer to the incident and scattered light, respectively. Two additional configurations with circular polarized incident light are denoted CV and CH. The HRS intensity at 90° scattering angle, with elliptical polarized light incident and linear polarized light detected, may be expressed in terms of the molecule-frame β tensor components as shown by Bersohn *et al.*[4] With the elliptical polarized incident electric field given by

$$\vec{E} = E_0[\hat{e}_V \cos\psi \cos(\omega t) + \hat{e}_H \sin\psi \cos(\omega t - \delta)], \quad (1)$$

the V and H linear polarized HRS scattered intensities are

$$I_{EV} = A\cos^4\psi + B\sin^4\psi + C\sin^2\psi\cos^2\psi, \quad (2)$$

$$I_{EH} = B\sin^4\psi + B\cos^4\psi + D\sin^2\psi\cos^2\psi. \quad (3)$$

Suppressing the common proportionality constant, the four coefficients A, B, C, D can be expressed in terms of six isotropic averages of lab-frame β tensor components[4]

$$A = \langle\beta_{ZZZ}^2\rangle = t_1, \quad (4)$$

$$B = \langle\beta_{ZYY}^2\rangle = t_2, \quad (5)$$

$$C = \langle(\beta_{ZYZ} + \beta_{ZZY})^2 + 2\beta_{ZZZ}\beta_{ZYY}\cos(2\delta)\rangle = t_5 + 2t_4\cos(2\delta), \quad (6)$$

$$D = \langle(\beta_{XYZ} + \beta_{XZY})^2 + 2\beta_{XZZ}\beta_{XYY}\cos(2\delta)\rangle = t_6 + 2t_3\cos(2\delta). \quad (7)$$

The six HRS intensities with V, H, or C incident polarization ($\delta = 90°$, $\psi = 0°$, 90°, or 45°, respectively) are given by

$$I_{VV} = t_1, \quad (8)$$

$$I_{HV} = I_{VH} = I_{HH} = t_2, \quad (9)$$

$$I_{CV} = (t_1 + t_2 - 2t_4 + t_5)/4, \quad (10)$$

$$I_{CH} = (2t_2 - 2t_3 + t_6)/4. \quad (11)$$

Expressions for the six terms $t_1 - t_6$ in Eqs. (8)–(11), for $C_{\infty v}$, C_{3v}, or C_{2v} point group symmetry, are[4]

$$t_1 = \langle \beta^2_{ZZZ} \rangle = (30a_1 + 12b_1 + 12b_2 + 6b_3 + 12b_4 + 6b_5 + 2g_1 + 2g_2 + 4g_3)/210, \quad (12)$$

$$t_2 = \langle \beta^2_{XZZ} \rangle = (6a_1 + 8b_1 - 6b_2 + 18b_3 - 6b_4 + 4b_5 + 6g_1 - g_2 - 2g_3)/210, \quad (13)$$

$$t_3 = \langle \beta_{XZZ}\beta_{XYY} \rangle = (2a_1 + 12b_1 - 2b_2 + 6b_3 - 2b_4 - b_5 + 16g_1 + 2g_2 - 10g_3)/210, \quad (14)$$

$$t_4 = \langle \beta_{ZZZ}\beta_{ZYY} \rangle = (6a_1 + 22b_1 + b_2 + 4b_3 + b_4 - 3b_5 + 6g_1 - g_2 + 5g_3)/210, \quad (15)$$

$$t_5 = \langle (\beta_{ZYZ} + \beta_{ZZY})^2 \rangle = (24a_1 - 24b_1 + 4b_2 + 16b_3 + 4b_4 + 16b_5 - 4g_1 + 3g_2 - 8g_3)/210, \quad (16)$$

$$t_6 = \langle (\beta_{XYZ} + \beta_{XZY})^2 \rangle = (8a_1 - 8b_1 - 8b_2 + 24b_3 - 8b_4 + 10b_5 - 20g_1 - 6g_2 + 16g_3)/210. \quad (17)$$

Table I gives expressions for the nine factors $a_1 - g_3$ in terms of the non-vanishing, independent, molecule-frame β tensor components for molecules with $C_{\infty v}$, C_{3v}, or C_{2v} point group symmetry.[4] There are 3, 4 or 5 independent β tensor components for molecules with $C_{\infty v}$, C_{3v}, or C_{2v} symmetry, respectively.[8] HRS measurements with VV, HV, CV, and CH polarizations can potentially determine four components. In the case that Kleinman symmetry holds (permutation symmetry of all the β spatial subscripts) the number of independent β tensor components is reduced to 2, 3 or 3, but then at most two components can be determined since all HRS observations at 90° scattering angle can be expressed in terms of just I_{VV} and I_{HV} (for example, $I_{CV} = 2I_{HV}$ and $6I_{CH} = 9I_{HV} - I_{VV}$). Kleinman symmetry, which is exact in the static limit, is not assumed in the analysis of the experimental measurements.

TABLE I. HRS intensity factors in Eqs. (12)–(17) expressed in terms of molecule-frame β tensor components, obtained using Eqs. (34)–(44) and Table I of Ref. 4. For $C_{\infty v}$ molecules $\beta_{yyy} = 0$. The last line gives results for $\beta_{||}$ measured by ESHG.

Factor	$C_{\infty v}$, C_{3v}	C_{2v}
a_1	$\beta^2_{zzz} + \beta^2_{yyy}$	β^2_{zzz}
b_1	$2\beta_{zzz}\beta_{zxx} - \beta^2_{yyy}$	$\beta_{zzz}(\beta_{zxx} + \beta_{zyy})$
b_2	$4\beta_{zzz}\beta_{xxz} - 2\beta^2_{yyy}$	$2\beta_{zzz}(\beta_{xxz} + \beta_{yyz})$
b_3	$2\beta^2_{zxx} + \beta^2_{yyy}$	$\beta^2_{zxx} + \beta^2_{zyy}$
b_4	$4\beta_{zxx}\beta_{xxz} + 2\beta^2_{yyy}$	$2(\beta_{zxx}\beta_{xxz} + \beta_{zyy}\beta_{yyz})$
b_5	$8\beta^2_{xxz} + 4\beta^2_{yyy}$	$4(\beta^2_{xxz} + \beta^2_{yyz})$
g_1	$2\beta^2_{zxx}$	$2\beta_{zxx}\beta_{zyy}$
g_2	$8\beta^2_{xxz}$	$2\beta_{xxz}\beta_{yyz}$
g_3	$4\beta_{zxx}\beta_{xxz}$	$2(\beta_{zxx}\beta_{yyz} + \beta_{zyy}\beta_{xxz})$
$5\beta_{||}$	$3\beta_{zzz} + 2\beta_{zxx} + 4\beta_{xxz}$	$3\beta_{zzz} + \beta_{zxx} + 2\beta_{xxz} + \beta_{zyy} + 2\beta_{yyz}$

For molecules with T_d point group symmetry, where β_{xyz} is the only non-vanishing independent tensor component, one has $I_{VV} = (12/35)\beta^2_{xyz}$, $I_{VV}/I_{HV} = 3/2$, $I_{CV}/I_{HV} = 2$, and $I_{CH}/I_{HV} = 5/4$.

III. HYPER-RAYLEIGH SCATTERING EXPERIMENT

The present HRS measurements were made with linear or circular polarized light at or near the 90° scattering angle, using previously described apparatus and techniques.[9] The main experimental measurements are the gas phase HRS intensity I_{VV}, and the polarization ratios I_{VV}/I_{HV}, I_{CV}/I_{HV}, and I_{CH}/I_{VH}.

The gas sample is contained in a 1 cm fused silica fluorometer cuvette sealed to a sample reservoir and fill valve. Six of the sample molecules (N_2O, NH_3, SO_2, CH_4, CF_4, CF_2Cl_2) were measured at room temperature (22°C) with 2 atm gas fill pressure. The less volatile samples [D_2O, CCl_4, $(CH_3)_2CO$] were measured with 2 atm vapour pressure set by the temperature of the liquid in the sample reservoir, and with the cuvette and the remainder of the sample assembly placed inside an oven which was set to a temperature 10°C higher to prevent condensation on the cuvette windows. Sample purity was >99.9% (except 99% for CF_2Cl_2).

The laser beam (λ = 1064 nm, 100 ns pulses, 4 kHz repetition rate, 2 W average power, multi-longitudinal mode, 0.5 cm^{-1} spectral width) was focused into the sample cuvette, with the laser beam waist placed precisely at the focus of the aspheric lens that collected the scattered light. The numerical aperture of the collection optics ($NA = \sin \alpha_C$, where α_C is the angular radius of the cone of light accepted by the collection optics) was controlled by an iris placed after the collection lens, and a 350 cm^{-1} spectral band centered at λ = 532 nm was selected by an interference filter placed before the detector. The HRS signals were in the range 0.01–20 photon counts/s, while the background due to the gated dark count rate of the photomultiplier detector was 0.001 s^{-1}. It is convenient to align the apparatus using CF_2Cl_2 since this gas gives a strong HRS signal and is easy to handle. A problem for some of the sample molecules was decomposition that occurred at the laser beam spot on the window, depositing a beam-absorbing or second harmonic generating spot. Significant sample degradation was observed in 1 min for CO and CH_3CN, in 10 min for acetone, and 1 h for CCl_4. No useful results could be obtained for CO and CH_3CN, and only limited results were obtained for acetone and CCl_4. Baking the cuvette in air at 800 °C for 1 h eliminated the background signal due to such window contamination. No degradation was observed for the other samples during laser beam exposure for days or weeks.

The polarization state of the incident laser beam was switched using a liquid crystal variable wave plate (LCVWP) while the scattered light polarization remained fixed. Each polarization ratio was determined from HRS photon counts recorded for two different polarization configurations, alternating between the two configurations at 10 s intervals for several hundred cycles. Special measures described in Appendix A were required to set the LCVWP for the CV polarization configuration. Polarization ratio measurements

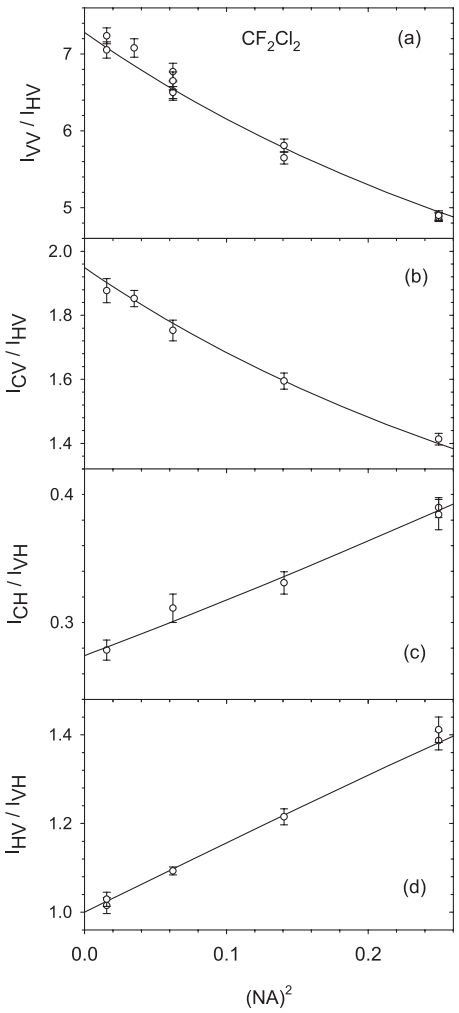

FIG. 1. HRS polarization ratio measurements for CF_2Cl_2 are shown by the open circles with error bars representing photon counting statistics, and the solid curves show the functions fit to the data as described in Appendix B. The fit parameters P^2, Q^2, and R^2 are the $NA = 0$ intercepts for the functions in (a), (b), and (c), respectively. The curve through the I_{HV}/I_{VH} data in (d) has no additional adjustable parameters and serves as a check.

were made for several values of the collection numerical aperture, and extrapolated to $NA = 0$ as shown in Figure 1 and described in Appendix B. The experimentally determined polarization ratios at $NA = 0$ are shown in Table II.

The normalized HRS signal measured in the VV polarization configuration is given by

$$S_{VV}(\mathrm{s^{-1}W^{-2}M^{-1}sr^{-1}}) = I_{VV}/(P^2\rho\,\Omega), \tag{18}$$

TABLE II. Experimental measurements of HRS polarization ratios.

Gas	Point group	I_{VV}/I_{HV}	I_{CV}/I_{HV}	I_{CH}/I_{VH}
CCl_4	T_d	1.55 ± 0.10		
N_2O	$C_{\infty V}$	5.95 ± 0.04	1.93 ± 0.03	0.484 ± 0.006
NH_3	C_{3V}	7.55 ± 0.05	1.78 ± 0.03	0.147 ± 0.004
D_2O	C_{2V}	8.02 ± 0.05	2.06 ± 0.04	0.185 ± 0.009
SO_2	C_{2V}	9.26 ± 0.15	2.25 ± 0.04	0.099 ± 0.007
CF_2Cl_2	C_{2V}	7.28 ± 0.04	1.95 ± 0.03	0.274 ± 0.004
$(CH_3)_2CO$	C_{2V}	5.17 ± 0.23		

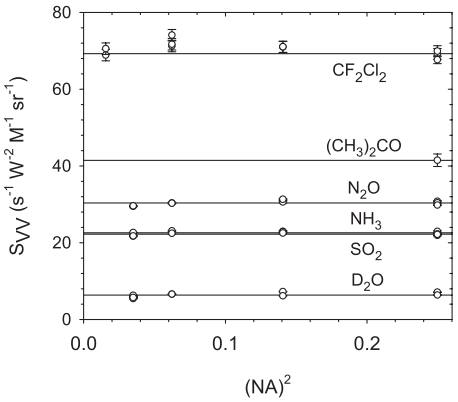

FIG. 2. Measurements of the normalized HRS signal S_{VV} are shown by the open circles with error bars representing photon counting statistics. The data for each molecule is adequately fit by a horizontal line.

where I_{VV} is the measured HRS signal intensity, P is the laser beam power, ρ is the gas number density determined from the measured gas pressure and temperature using the virial equation of state,[10] and $\Omega = 2\pi(1 - \cos[\arcsin(NA)])$ is the collection solid angle. The normalized HRS signal S_{VV} is found to be independent of NA to within the experimental uncertainty, as shown by the horizontal lines fitted to the data for each molecule in Figure 2, and measurements made over several months were reproducible to $\pm 3\%$. Table III gives the average S_{VV} measured for each molecule.

IV. EXPERIMENTAL RESULTS

Symmetry determines the HRS polarization ratios for the T_d molecules. As a check, I_{VV}/I_{HV} for CCl_4 was measured, and the result in Table II agrees with the expected value.

The HRS polarization ratios I_{VV}/I_{HV}, I_{CV}/I_{HV}, and I_{CH}/I_{VH} were measured for the five molecules N_2O, NH_3, D_2O, SO_2, and CF_2Cl_2, as shown in Table II, and for these molecules one may use Eqs. (8)–(17) and Table I to solve for sets of β tensor component ratios consistent with the observed HRS polarization ratios. The results are shown in Table IV. There is a sharply defined solution for the $C_{\infty v}$ molecule N_2O, but for each of the other four molecules a wide range of solutions fit the observations. For these four molecules a typical solution is shown, as well as the range of possible values found for each tensor component ratio.

TABLE III. Experimental measurements of normalized HRS signal and first hyperpolarizability.

Gas	S_{VV} ($\mathrm{s^{-1}\ W^{-2}\ M^{-1}\ sr^{-1}}$)	β_{VV} (a.u.)
CH_4	2.00 ± 0.08	5.9 ± 0.4
CF_4	1.03 ± 0.02	4.2 ± 0.3
CCl_4	5.7 ± 0.1	9.9 ± 0.8
N_2O	30.4 ± 0.6	22.8 ± 1.7
NH_3	22.6 ± 0.5	19.7 ± 1.5
D_2O	6.3 ± 0.2	10.4 ± 0.7
SO_2	22.3 ± 0.5	19.6 ± 1.5
CF_2Cl_2	69.3 ± 1.6	34.5 ± 2.7
$(CH_3)_2CO$	41 ± 2	26.5 ± 2.4

TABLE IV. Ratios of β tensor component consistent with the observed HRS polarization ratios. A unique solution is obtained for N_2O. For the other molecules, the first line gives a typical solution, and the second line in brackets gives the range of values obtained.

Gas	β_{zxx}/β_{zzz}	β_{zyy}/β_{zxx}	β_{xxz}/β_{zxx}	β_{yyz}/β_{zyy}	β_{yyy}/β_{zzz}	$\beta_{\|\|}/\beta_{VV}$
N_2O	0.058 ± 0.002		0.91 ± 0.02			1.645 ± 0.001
NH_3	0.20		0.92		0.07	1.712 ± 0.001
	[0.18–0.61]		[0.90–0.96]		[0.00–0.20]	
D_2O	0.65	0.53	1.01	1.02		1.708 ± 0.001
	[0.16–0.72]	[0.21–1.00]	[0.89–1.02]	[1.01–1.47]		
SO_2	0.45	0.60	1.12	0.97		1.722 ± 0.002
	[0.23–0.56]	[0.34–1.00]	[0.85–1.27]	[0.74–1.88]		
CF_2Cl_2	0.15	0.71	0.98	0.98		1.694 ± 0.002
	[0.14–0.23]	[0.23–1.00]	[0.57–1.38]	[0.5–2.0]		

Table II shows significant deviations from $I_{CV}/I_{HV} = 2$ for all five molecules for which it was measured, with NH_3 and SO_2 showing the largest deviations. The deviation from $I_{CV}/I_{HV} = 2$ indicates that Kleinman symmetry does not hold, and the ratio $I_{VV}/I_{HV} > 9$ is a second indicator of Kleinman symmetry breaking in the case of SO_2. Kleinman symmetry breaking for N_2O and NH_3 is due to the inequality of just one pair of components, β_{zxx} and β_{xxz}. Table IV shows that the ratio of these components is well determined for these molecules, and their difference is about 10%. For D_2O, SO_2, and CF_2Cl_2, where there are two pairs of tensor components affected by Kleinman symmetry breaking, there are many solutions consistent with the HRS observations and the tensor component ratios are not well determined. However, the typical solutions in Table IV for these molecules show that the observed deviations from $I_{CV}/I_{HV} = 2$ can be accounted for by small deviations from Kleinman symmetry for the tensor components.

The last column of Table IV shows $\beta_{||}/\beta_{VV}$, where $\beta_{VV} = \langle\beta^2_{ZZZ}\rangle^{1/2} \propto (I_{VV})^{1/2}$, evaluated using sets of β tensor components consistent with the HRS observations. The error bar on $\beta_{||}/\beta_{VV}$ indicates the entire range of values consistent with the HRS observations, and one sees that $\beta_{||}/\beta_{VV}$ is very accurately determined despite large uncertainties for the β tensor components. This enables one to calibrate β_{VV} using ESHG measurements of $\beta_{||}$. In particular, one obtains $\beta_{VV} = 10.4 \pm 0.7$ a.u. (atomic units) for D_2O using the previous ESHG measurement $\beta_{||} = -17.8 \pm 1.2$ a.u. at $\lambda = 1064$ nm for calibration.[11] (The gas phase ESHG measurement for D_2O was calibrated against N_2,[12] which was ultimately calibrated by the *ab initio* calculation for He.[13]) Then, one may apply $\beta^A_{VV}/\beta^B_{VV} = (S^A_{VV}/S^B_{VV})^{1/2}$ to calibrate β_{VV} for the other molecules. The β_{VV} values so obtained are shown in the third column of Table III.

This calibration assumes that the measured S_{VV} includes the entire rotational HRS spectrum, which is a potential problem for the light molecules CH_4, NH_3, and D_2O. The HRS spectrum for CH_4 has been calculated as previously described,[14] and it is found that 74% of the integrated HRS intensity falls within a 350 cm^{-1} wide spectral window centered at the second harmonic frequency. The result $S_{VV} = 2.00 \pm 0.08 = (1.48 \pm 0.06)/0.74$ in Table III takes this into account. In the case of D_2O the observed rotational Raman spectrum extends past 300 cm^{-1} on the Stokes side,[15] and the HRS spectrum which also includes transitions with $\Delta J = \pm 3$ will extend even further.[16] However, $I_{VV}/I_{HV} = 8.02$ for D_2O indicates that the vector part of β dominates, so transitions with $\Delta J = 0, \pm 1$ will make the main contribution to the HRS spectrum, with width similar to that of the rotational bandwidth (<300 cm^{-1}) of the infrared absorption spectrum.[17] It has been assumed that the entire rotational HRS spectrum is included in the S_{VV} measurement for D_2O and also for NH_3. If only a fraction F of the D_2O HRS spectral intensity falls within the 350 cm^{-1} measurement bandwidth, then the β_{VV} values calibrated against D_2O in Table III are overestimates by a factor $F^{-1/2}$. This issue could be resolved by a measurement or calculation of the D_2O HRS spectrum.

For the tetrahedral molecules CH_4, CF_4, and CCl_4 the experimental β_{VV} value immediately determines the single independent component $\beta_{xyz} = (35/12)^{1/2}\beta_{VV}$, which is given in the last column of Table V. The previously measured β_{xyz} values for CH_4, CF_4, and CCl_4 in the gas phase (7.1 ± 0.9, 5.4 ± 0.6, and 11.0 ± 0.9, respectively) (Ref. 14) are lower by a factor 0.7 compared to the present results, but they are less reliable since the calibration of the previous results was indirect and involved liquid phase HRS intensities.

V. COMPARISON WITH *AB INITIO* CALCULATIONS

The *ab initio* β_{xyz} values for the tetrahedral molecules CH_4, CF_4, and CCl_4, calculated at the experimental laser frequency and including electronic (β^e), zero-point vibrational averaging (β^{ZPVA}) and pure vibrational (β^v) contributions, are shown in Table V for comparison with the experimental results.[18] The vibrational terms nearly cancel, making a small net contribution to the total. For CH_4 the *ab initio* result

TABLE V. Comparison of calculated (MP2) (Ref. 18) and experimental β_{xyz}(a.u.) for CX_4 molecules.

Gas	β^e_{xyz} Calc.	β^{ZPVA}_{xyz} Calc.	β^v_{xyz} Calc.	β_{xyz} Calc.	$\|\beta_{xyz}\|$ Expt.
CH_4	− 8.77	−1.21	+0.81	−9.2	10.0 ± 0.7
CF_4	4.16–6.1	−0.13	+0.31	4.3–6.3	7.2 ± 0.5
CCl_4	9.7–14.7	−1.53	+0.47	8.6–13.6	16.9 ± 1.4

TABLE VI. Comparison of calculated β^e(a.u.) [static, CCSD(T), 162 CGTF basis] (Ref. 20) and experimental β(a.u.) for N_2O.

N_2O	Calc.	Expt.
β_{zzz}	53.1	56.3 ± 4.2
β_{zxx}	3.3	3.3 ± 0.3
β_{xxz}	3.3	3.0 ± 0.3
β_{zxx}/β_{zzz}	0.062	0.058 ± 0.002
β_{xxz}/β_{zxx}	1	0.91 ± 0.02
$\beta_{\|\|}$	35.8	37.5 ± 2.8
β_{VV}	21.7	22.8 ± 1.7
$\beta_{\|\|}/\beta_{\mathrm{HRS}}$	1.651	1.645 ± 0.001
I_{VV}/I_{HV}	6.19	5.95 ± 0.04
I_{CV}/I_{HV}	2	1.93 ± 0.03
I_{CH}/I_{VH}	0.468	0.484 ± 0.006

TABLE VII. Comparison of calculated β^e(a.u.) [static, CCSD(T), 168 CGTF basis] (Ref. 21) and experimental β(a.u.) for SO_2.

SO_2	Calc.	Expt.
β_{zzz}	29.7	
β_{zxx}	12.6	
β_{zyy}	8.0	
β_{zxx}/β_{zzz}	0.424	0.45 [0.23–0.56]
β_{zyy}/β_{zxx}	0.635	0.60 [0.34–1.00]
$\beta_{\|\|}$	30.2	33.8 ± 2.6
β_{VV}	17.5	19.6 ± 1.5
$\beta_{\|\|}/\beta_{VV}$	1.727	1.722 ± 0.002
I_{VV}/I_{HV}	8.74	9.26 ± 0.15
I_{CV}/I_{HV}	2	2.25 ± 0.04
I_{CH}/I_{VH}	0.044	0.099 ± 0.007

TABLE VIII. *Ab initio* electronic hyperpolarizabilities β^e (a.u.) for H_2O.

H_2O	ω (a.u.)	a	b	c	d	e	f	g	h
$-\beta_{zzz}$	0	14.67	16.3	13.18	13.97	13.77	13.3	15.1	12.10
	0.04282			14.22	15.12				
	0.06562			15.84	16.93			17.5	14.50
$-\beta_{zxx}$	0	9.95	9.8	9.03	9.92	9.80	10.0	11.1	8.93
	0.04282			9.60	10.53				
	0.06562			10.47	11.47			12.4	10.25
$-\beta_{xxz}$	0	9.95	9.8	9.03	9.92	9.80	10.0	11.1	8.93
	0.04282			9.56	10.50				
	0.06562			10.34	11.36			12.2	10.18
$-\beta_{zyy}$	0	5.88	6.1	5.17	5.66	5.61	4.4	6.2	5.11
	0.04282			5.48	6.07				
	0.06562			5.93	6.68			6.6	5.83
$-\beta_{yyz}$	0	5.88	6.1	5.17	5.66	5.61	4.4	6.2	5.11
	0.04282			5.98	6.65				
	0.06562			7.43	8.48			9.3	7.59
$-\beta_{\|\|}$	0	18.30	19.32	16.43	17.73	17.51	16.60	19.4	15.68
	0.04282			17.76	19.25				
	0.06562			19.89	21.72			22.9	19.0
β_{VV}	0	10.72	11.27	9.63	10.41	10.28	9.82	11.43	9.22
	0.04282			10.40	11.29				
	0.06562			11.63	12.71			13.43	11.16
$-\beta_{\|\|}/\beta_{VV}$	0	1.707	1.715	1.706	1.703	1.703	1.693	1.700	1.700
	0.04282			1.708	1.706				
	0.06562			1.710	1.709			1.706	1.705
I_{VV}/I_{HV}	0	7.87	8.20	7.83	7.73	7.72	7.37	7.62	7.62
	0.04282			8.26	8.20				
	0.06562			9.02	9.09			9.37	9.06
I_{CV}/I_{HV}	0	2	2	2	2	2	2	2	2
	0.04282			2.14	2.15				
	0.06562			2.40	2.44			2.63	2.50
I_{CH}/I_{VH}	0	0.189	0.133	0.196	0.212	0.213	0.272	0.231	0.230
	0.04282			0.192	0.208				
	0.06562			0.195	0.212			0.256	0.241

[a]Reference 2, CCSD, q-aug-cc-pVQZ rank 343 basis.
[b]Reference 1, MP4-SDTQ, W1 [6*s*4*p*3*d*1*f* /4*s*3*p*1*d*] basis.
[c]Reference 22, QED-MP2, d-aug-cc-pVTZ [6*s*5*p*4*d*3*f* /5*s*4*p*3*d*] basis.
[d]Reference 23, CCSD, d-aug-cc-pVTZ basis.
[e]Reference 24, CCSD(T), KT1 [9*s*6*p*6*d*3*f* /6*s*4*p*2*d*1*f*] 148 CGTF basis.
[f]Reference 25, DFT LB94.
[g]Reference 26, MCSCF.
[h]Reference 27, MCSCF, CAS1, P3 basis.

TABLE IX. *Ab initio* vibrational hyperpolarizabilities β^{ZPVA} (a.u.) and β^{v}(a.u.) for H_2O. Results for D_2O are in parentheses.

H_2O	ω (a.u.)	β^{ZPVA} [a]	β^{ZPVA} [b]	β^{ZPVA} [c]	β^{v} [b]	β^{v} [c]
$-\beta_{zzz}$	0		0.655	0.671	− 2.340	− 3.985
	0.07				0.146	
$-\beta_{zxx}$	0		1.069		− 0.757	
	0.07				0.230	
$-\beta_{xxz}$	0		1.069		− 0.757	
	0.07				0.174	
$-\beta_{zyy}$	0		− 0.145		0.643	
	0.07				0.003	
$-\beta_{yyz}$	0		− 0.145		0.643	
	0.07				0.015	
$-\beta_{\|\|}$	0	1.38(1.10)	0.947		− 1.47	
	0.06562	1.83(1.45)				
	0.07				0.21	

[a]Reference 27, MCSCF.
[b]Reference 28, MP2, [5*s*3*p*2*d*/3*s*2*p*] basis.
[c]Reference 29, FVCI.

shown in Table V is thought to have converged within 0.3 a.u., based on comparison with another calculation that thoroughly investigated basis set and correlation effects for the static electronic hyperpolarizability at the equilibrium geometry,[19] and the experimental and theoretical β_{xyz} results for CH_4 in Table V are in agreement. For CF_4 and CCl_4 the convergence of the calculations is incomplete and the calculated values fall below the experimental results.

Tables VI and VII compare the HRS experimental results for N_2O and SO_2 with the results from recent *ab initio* calculations of static β^e for these molecules using CCSD(T) correlation treatment and large basis sets (162 and 168 CGTF).[20,21] The small quantitative differences between experiment and calculation for these molecules (5% for N_2O, 10% for SO_2) may be ascribed to neglect of frequency dispersion and vibrational contributions in the comparison. For the C_{2V} molecules the z axis is the twofold axis, pointing in the direction of the permanent molecular dipole moment, and xz has been chosen as the molecular plane. Since the calculations give $\beta_{zxx} > \beta_{zyy}$, the larger off-diagonal component obtained from the analysis of the HRS measurements has been assigned as β_{zxx}. Comparable *ab initio* calculations are not available for CF_2Cl_2 and $(CH_3)_2CO$.

Table VIII shows the results of electron correlated *ab initio* calculations for the H_2O β^e tensor, at the equilibrium geometry, both in the static limit and at the optical frequencies for nonlinear optical measurements (ω = 0, 0.04282, and 0.06562 a.u., corresponding to $\lambda = \infty$, 1064, and 694.3 nm).[1,2,22–27] Table IX shows results of *ab initio* calculations of β^{ZPVA} and β^{v} for H_2O (at $\omega = 0$ and 0.07 a.u.).[27–29] (Note that yz is the molecular plane in Refs. 22, 23, 27, and 28.) The β^e values from different calculations in Table VIII vary over a 20% range, and the calculated polarization ratios vary 10%. The β^{ZPVA} and β^{v} results from different calculations in Table IX differ as much as 40%. The values for static β^{v}_{zzz} calculated using both the double perturbation theory approach of Bishop and Kirtman (BK) (Ref. 28) and the more recent vibrational configuration interaction (VCI) approach[29] differ by 40%. Table X gives theoretical results for D_2O at ω = 0.04282 a.u. constructed using the data in Tables VIII and IX. The results for β^e at the equilibrium geometry are from Ref. 22, while β^{ZPVA} and β^{v} are scaled values from Ref. 28. The scaling β^{ZPVA} (D_2O, ω = 0.04282 a.u.) = 0.86 × β^{ZPVA} (H_2O, ω = 0 a.u.) is based on $\beta^{ZPVA}_{||}$ (H_2O)/$\beta^{ZPVA}_{||}$ (D_2O) = 1.26 from Ref. 27, and the H_2O $\beta^{e}_{||}$ frequency dispersion from Refs. 22 and 23. The scaling β^{v} (D_2O, ω = 0.04282 a.u.) = 2.0 × β^{v} (H_2O, ω = 0.07 a.u.) assumes $\beta^{v} \propto \nu_0/(\nu^2 - \nu_0^2)$, which describes the response for frequencies far from a single dominant vibrational resonance. The average of the ν_1, ν_2 and ν_3 fundamental vibration frequencies[30] gives the estimate ν_0 = 3003 cm^{-1} for H_2O and 2213 cm^{-1} for D_2O. There are several significant disagreements between

TABLE X. Comparison of calculated and experimental β (a.u.) for D_2O at ω = 0.04282 a.u.

D_2O	β^e Calc.	β^{ZPVA} Calc.	β^{v} Calc.	β Calc.	β Expt.
$-\beta_{zzz}$	14.22	0.56	0.29	15.07	
$-\beta_{zxx}$	9.60	0.92	0.46	10.975	
$-\beta_{xxz}$	9.56	0.92	0.35	10.83	
$-\beta_{zyy}$	5.48	− 0.13	0.01	5.36	
$-\beta_{yyz}$	5.98	− 0.13	0.03	5.89	
$-\beta_{\|\|}$	17.76			19.00	17.8 ± 1.2
β_{VV}	10.40			11.17	10.4 ± 0.7
$-\beta_{\|\|}/\beta_{VV}$	1.708			1.701	1.708 ± 0.001
I_{VV}/I_{HV}	8.26			7.89	8.02 ± 0.05
I_{CV}/I_{HV}	2.14			2.10	2.06 ± 0.04
I_{CH}/I_{VH}	0.192			0.238	0.185 ± 0.009

TABLE XI. *Ab initio* electronic hyperpolarizabilities β^e (a.u.) for NH_3.

NH_3	ω (a.u.)	[a]	[b]	[c]
$-\beta_{zzz}$	0	37.93	30.7	34.02
	0.06562	58.27		
$-\beta_{zxx}$	0	8.23	10.0	8.38
	0.06562	12.82		
$-\beta_{xxz}$	0	8.23	10.0	8.38
	0.06562	11.34		
$-\beta_{yyy}$	0	6.91	8.20	7.83
	0.06562	8.14		
$-\beta_{\|\|}$	0	32.64	30.42	30.47
	0.06562	49.16		
β_{VV}	0	19.24	18.00	18.03
	0.06562	28.85		
$-\beta_{\|\|}/\beta_{VV}$	0	1.697	1.690	1.689
	0.06562	1.704		
I_{VV}/I_{HV}	0	7.49	7.27	7.24
	0.06562	7.02		
I_{CV}/I_{HV}	0	2	2	2
	0.06562	1.72		
I_{CH}/I_{VH}	0	0.252	0.288	0.293
	0.06562	0.190		

[a]Reference 22, QED-MP2, mHyPOL [5*s*3*p*3*d*2*f* /3*s*3*p*2*d*] basis.
[b]Reference 25, DFT LB94.
[c]Reference 31, SDQ-MP4, [6*s*4*p*4*d*1*f* /4*s*2*p*1*d*] basis.

TABLE XII. *Ab initio* vibrational hyperpolarizabilities β^{ZPVA} (a.u.) and β^{v} (a.u.) for NH_3.

NH_3	ω (a.u.)	β^{ZPVA} [a]	β^{ZPVA} [b,c]	β^{v} [a]	β^{v} [b,c]
$-\beta_{zzz}$	0	0.518	−0.8	156.6	235.5
	0.07			−0.150	
$-\beta_{zxx}$	0	1.678		−0.531	
	0.07			0.048	
$-\beta_{xxz}$	0	1.678		−0.531	
	0.07			−0.001	
$-\beta_{yyy}$	0	1.259		0.725	
	0.07			0.044	
$-\beta_{\|\|}$	0	2.324		93.35	
	0.07			−0.072	

[a]Reference 28, SCF (II).
[b]Reference 29, FVCI.
[c]Reference 32, 1D.

the theoretical and experimental results for D_2O in Table X, but only one is >10%. The discrepancy between experiment and theory is increased by inclusion of the vibrational contributions, and would be further increased if the β^e values in Table X were increased 10% as suggested by comparison of the static values from the five highest level calculations (a-e) in Table VIII.

Tables XI and XII show *ab initio* results for electronic (β^e) (Refs. 22, 25, and 31) and vibrational (β^{ZPVA} and β^{v}) (Refs. 28, 29, and 32) contributions for NH_3, respectively. Table XIII compares the theoretical and HRS experimental results. The theoretical results for β^e at $\omega = 0.04282$ a.u. are obtained from the Ref. 22 data given in Table XI by quadratic interpolation, $\beta(\omega_2) = \beta(0) + [\beta(\omega_1) - \beta(0)](\omega_2/\omega_1)^2$, while the values for β^{ZPVA} and β^{v} in Table XIII are scaled values from Ref. 28. The scaling $\beta^{ZPVA}(\omega = 0.04282 \text{ a.u.}) = 1.05 \times \beta^{ZPVA}(\omega = 0 \text{ a.u.})$ assumes the same dispersion as $\beta^e_{||}$, and the scaling $\beta^{v}(\omega = 0.04282 \text{ a.u.}) = 2.7 \times \beta^{v}(\omega = 0.07 \text{ a.u.})$ assumes $\beta^{v} \propto \nu_0/(\nu^2 - \nu_0^2)$, where $\nu_0 = 0.79$ cm^{-1} is the frequency for the inversion mode which dominates the vibrational contribution.[32] This large amplitude anharmonic umbrella vibration for NH_3 makes a huge contribution to β^{v}_{zzz} at $\omega = 0$, and the BK and VCI calculations differ by 50% for this component, but the β^{v} contributions are small at optical frequencies. The different calculations for β^{ZPVA} do not even agree on the sign. Including vibrational contributions β^{ZPVA} and β^{v} for NH_3 in Table XIII increases the discrepancy between theory and experiment for $\beta_{||}$ and β_{VV} from 18% to 25%.

TABLE XIII. Comparison of calculated and experimental β(a.u.) for NH_3 at $\omega = 0.04282$ a.u.

NH_3	β^e Calc.	β^{ZPVA} Calc.	β^{v} Calc.	β Calc.	β Expt.
$-\beta_{zzz}$	46.59	0.54	−0.41	46.73	
$-\beta_{zxx}$	10.19	1.76	0.13	12.08	
$-\beta_{xxz}$	9.56	1.76	0.00	11.32	
$-\beta_{yyy}$	7.44	1.32	0.12	8.88	
β_{zxx}/β_{zzz}	0.219			0.258	0.20 [0.18–0.61]
β_{xxz}/β_{zxx}	0.938			0.937	0.92 [0.90–0.96]
β_{yyy}/β_{zzz}	0.160			0.190	0.07 [0.00–0.20]
$-\beta_{\|\|}$	39.67			41.92	33.7 ± 2.6
β_{VV}	23.33			24.64	19.7 ± 1.5
$-\beta_{\|\|}/\beta_{VV}$	1.701			1.701	1.712 ± 0.001
I_{VV}/I_{HV}	7.25			7.22	7.55 ± 0.05
I_{CV}/I_{HV}	1.85			1.83	1.78 ± 0.03
I_{CH}/I_{VH}	0.216			0.211	0.147 ± 0.004

VI. SUMMARY AND CONCLUSION

Gas phase HRS measurements provide data which may be used to test *ab initio* calculations of molecular hyperpolarizabilities. Accurate absolute calibration of HRS β_{VV} for several molecules was achieved using ESHG $\beta_{||}$ measured at the same laser frequency for one of the molecules, and the measured HRS polarization ratios give information about the shape of the β tensor and deviations from Kleinman symmetry. All β tensor components can be accurately determined experimentally for molecules with T_d or $C_{\infty v}$ symmetry, where there are at most three independent nonvanishing components. For molecules of lower symmetry, where one cannot directly compare the experimental and theoretical β tensor components, the measured values for $\beta_{||}$, β_{VV}, I_{VV}/I_{HV}, I_{CV}/I_{HV} and I_{CH}/I_{VH} are compared against the corresponding values obtained from the calculated tensor components. Differences about 10% are seen for most of the comparisons between theory and experiment, even for high level *ab initio* calculations. Definitive comparisons are possible for the CX_4 molecules, where both electronic and vibrational contributions were calculated for several frequencies, and simple interpolation gives values directly comparable with experiment. This is not the case for the other molecules, where vibrational hyperpolarizability and electronic hyperpolarizability dispersion results are limited (H_2O, NH_3) or non-existent.

APPENDIX A: RETARDATION SENSITIVITY

The HRS polarization ratio I_{CV}/I_{HV} is very sensitive to small deviations from circular polarization for the incident beam. One finds that the derivatives of Eqs. (2) and (3) with respect to ψ and δ vanish at $\delta = \pi/2$ and $\psi = 0, \pi/4$, or $\pi/2$, except for

$$[dI_{EV}/d\psi]_{\psi=\pi/4} = (A - B). \tag{A1}$$

For $I_{EV} \approx I_{CV}$ one has

$$\left[\frac{dI_{EV}/d\psi}{I_{HV}}\right]_{\psi=\pi/4} = (A/B) - 1 = I_{VV}/I_{HV} - 1, \tag{A2}$$

so the error in I_{CV}/I_{HV} due to a small error $\Delta\psi$ in setting $\psi = \pi/4$ will be

$$\Delta(I_{CV}/I_{HV}) = (I_{VV}/I_{HV} - 1)\Delta\psi. \tag{A3}$$

The polarization state of the incident light is controlled by passing vertical polarized light through a LCVWP, with optic axis at angle $\pi/4$ to the vertical, and retardation Γ. The transmitted polarization has the form given by Eq. (1) with $\delta = \pi/2$ and $\psi = \Gamma/2$.

For $I_{VV}/I_{HV} = 9$ and $I_{CV}/I_{HV} = 2$, a 1% error in I_{CV}/I_{HV} will result from a retardation error $\Delta\Gamma = 2\Delta\psi = 5$ mrad ($= 0.3^\circ = \lambda/1200$). The retardation Γ may be measured and set with the required accuracy by inserting a linear polarizer after the LCVWP and measuring the transmission of the laser beam through the polarizer. The polarizer axis is first set V and then H, and from the transmission ratio

$$T_H/T_V = \tan^2(\Gamma/2) = \tan^2(\pi/4 + \Delta\psi) \tag{A4}$$

one obtains

$$\Delta\psi = \arctan[(T_H/T_V)^{1/2}] - \pi/4 \approx (1/4)(T_H/T_V - 1). \tag{A5}$$

Adjusting the LCVWP to give <1% deviation from $T_H/T_V = 1$ reduces the error in I_{CV}/I_{HV} to <0.5%.

APPENDIX B: FINITE COLLECTION APERTURE

Light collection over a large angular aperture is usually required to obtain adequate HRS signal, and this modifies the observed HRS polarization dependence. Normalized to I_{VH} for 90° scattering, the HRS intensities for V or H polarized scattered light in the direction (θ, ϕ) are[4]

$$I_{VV} = P^2\cos^2\phi + \sin^2\phi, \tag{B1}$$

$$I_{HV} = P^2\sin^2\theta\sin^2\phi + \cos^2\theta\sin^2\phi + \cos^2\phi, \tag{B2}$$

$$I_{CV} = Q^2(\sin^2\theta\sin^2\phi + \cos^2\phi) + R^2\cos^2\theta\sin^2\phi, \tag{B3}$$

$$I_{VH} = 1, \tag{B4}$$

$$I_{HH} = P^2\cos^2\theta + \sin^2\theta, \tag{B5}$$

$$I_{CH} = Q^2\cos^2\theta + R^2\sin^2\theta, \tag{B6}$$

where θ is the azimuthal angle around the vertical axis, measured from the incident beam direction in the nominal horizontal scattering plane, and ϕ is the angle above the horizontal plane. The observed signal is obtained by integration over a circular aperture centered on the collection optics axis ($\theta_0 = 90^\circ$, $\phi_0 = 0^\circ$). Cartesian coordinates (x, y) for points in the aperture are connected to the polar coordinates (θ, ϕ) by an equatorial orthogonal projection

$$\phi = \arcsin(y/R), \tag{B7}$$

$$\theta = \theta_0 + \arcsin[(x/R)/\cos\phi], \tag{B8}$$

where $r/R \le \sin\alpha_C = NA$ for points in the aperture, $r^2 = x^2 + y^2$ gives the distance from the center of the aperture, and the solid angle integration element is $d\Omega = dxdy/\cos[\arcsin(r/R)]$.

Due to two oblique reflections at the cuvette window and collimation of the collected light before the analyzing polarizer, there is a small polarization rotation of the scattered light

$$\Delta\alpha = \arctan\{[T_{TE}/T_{TM}]\sin\phi\sin(\theta - \theta_0)/[\cos\phi + \cos(\theta - \theta_0)]\}, \tag{B9}$$

where T_{TE} (T_{TM}) is the Fresnel intensity transmission coefficient for light with electric field polarized perpendicular (parallel) to the plane of incidence. The maximum rotation angle at the edge of the aperture is 4° for $NA = 0.5$ collection optics, and this polarization rotation mixes the V and H polarized HRS contributions.

The collected light is coupled into an optical fiber which carries the light to the detector. The small size of the fiber core discriminates against stray light but also requires precise focusing of the HRS source. The focusing of the HRS source is done using the largest aperture, and the best focus is determined by the light passing through the outer zone which has most of the area, while light through the smaller central zone of the aperture will be out of focus due to spherical aberration. The decreased coupling into the fiber core due to defocusing is represented using a radial-varying effective transmission $T(r)$ for the aperture.

The observed HRS intensities are obtained by integrating over the collection aperture

$$I_{EV}(NA) = \int dxdy\,[I_{EV}(\theta,\phi)\cos^2\Delta\alpha + I_{EH}(\theta,\phi)\sin^2\Delta\alpha]\,T(r)/\cos[\arcsin(r/R)], \tag{B10}$$

$$I_{EH}(NA) = \int dxdy\,[I_{EH}(\theta,\phi)\cos^2\Delta\alpha + I_{EV}(\theta,\phi)\sin^2\Delta\alpha]\,T(r)/\cos[\arcsin(r/R)]. \tag{B11}$$

The numerical aperture NA of the collection optics is determined using the measured diameters for the set of apertures and a ray trace of the optics. The accuracy of the NA values was confirmed using a quartz-tungsten-halogen lamp and integrating sphere Lambertian source which gave (detected signal)/$(NA)^2$ constant within about 1% (the lens aberrations do not affect the signal measured with the Lambertian source). An effective transmission $T(r)$ that increases 10% from center to edge for the largest aperture produces a normalized HRS signal S_{VV} independent of NA, in agreement with the HRS observations. The functions $I_{EV}(NA)$ and $I_{EH}(NA)$ are completely determined once the sample dependent parameters P^2, Q^2 and R^2 appearing in Eqs. (B1)–(B6) are specified.

The parameter P^2 is determined by adjusting P^2 to obtain the best fit of the calculated curve $I_{VV}(NA)/I_{HV}(NA)$ to the experimental data for I_{VV}/I_{HV} versus $(NA)^2$, and the parameters Q^2 and R^2 are similarly determined from fits to the I_{CV}/I_{HV} and I_{CH}/I_{VH} data. The parameters P^2, Q^2, and R^2 are the values at $\theta = 90^\circ$ and $NA = 0$ for the polarization ratios I_{VV}/I_{HV}, I_{CV}/I_{HV}, and I_{CH}/I_{VH}.

[1] A. V. Gubskaya and P. G. Kusalik, Mol. Phys. **99**, 1107 (2001).
[2] J. R. Hammond and K. Kowalski, J. Chem. Phys. **130**, 194108 (2009).
[3] D. P. Shelton and J. E. Rice, Chem. Rev. **94**, 3 (1994).
[4] R. Bersohn, Y.-H. Pao, and H. L. Frisch, J. Chem. Phys. **45**, 3184 (1966).
[5] P. D. Maker, Phys. Rev. A **1**, 923 (1970).
[6] M. Kauranen and A. Persoons, J. Chem. Phys. **104**, 3445 (1996).
[7] V. Ostroverkhov, R. G. Petschek, K. D. Singer, L. Sukhomlinova, R. J. Tweig, S.-X. Wang, and L. C. Chien, J. Opt. Soc. Am. B **17**, 1531 (2000).

[8]P. N. Butcher and D. Cotter, *The Elements of Nonlinear Optics* (Cambridge University Press, Cambridge, 1990).
[9]D. P. Shelton, Rev. Sci. Instrum. **82**, 113103 (2011).
[10]J. H. Dymond and E. B. Smith, *The Virial Coefficients of Pure Gases and Mixtures* (Clarendon, Oxford, 1980).
[11]P. Kaatz, E. A. Donley, and D. P. Shelton, J. Chem. Phys. **108**, 849 (1998).
[12]D. P. Shelton, Phys. Rev. A **42**, 2578 (1990).
[13]D. M. Bishop and J. Pipin, J. Chem. Phys. **91**, 3549 (1989).
[14]R. D. Pyatt and D. P. Shelton, J. Chem. Phys. **114**, 9938 (2001).
[15]G. Avila, G. Tejeda, J. M. Fernandez, and S. Montero, J. Mol. Spectrosc. **220**, 259 (2003).
[16]S. Kielich, Prog. Opt. **20**, 155 (1983).
[17]E. F. Barker and W. W. Sleator, J. Chem. Phys. **3**, 660 (1935).
[18]D. M. Bishop, F. L. Gu, and S. M. Cybulski, J. Chem. Phys. **109**, 8407 (1998).
[19]G. Maroulis, Chem. Phys. Lett. **226**, 420 (1994).
[20]G. Maroulis and M. Menadakis, Chem. Phys. Lett. **494**, 144 (2010).
[21]D. Xenides and G. Maroulis, Chem. Phys. Lett. **319**, 618 (2000).
[22]T. Kobayashi, F. Aiga, and K. Yamaguchi, J. Chem. Phys. **110**, 11720 (1999).
[23]O. Christiansen, J. Gauss, and J. Stanton, Chem. Phys. Lett. **305**, 147 (1999).
[24]G. Maroulis, Chem. Phys. Lett. **289**, 403 (1998).
[25]S. J. A. van Gisbergen, J. G. Snijders, and E. J. Baerends, J. Chem. Phys. **109**, 10657 (1998).
[26]D. Spelsberg and W. Meyer, J. Chem. Phys. **108**, 1532 (1998).
[27]Y. Luo, H. Agren, O. Vahtras, P. Jorgensen, V. Spirko, and H. Hettema, J. Chem. Phys. **98**, 7159 (1993).
[28]D. M. Bishop, B. Kirtman, H. A. Kurtz, and J. E. Rice, J. Chem. Phys. **98**, 8024 (1993).
[29]J. M. Luis, M. Torrent-Sucarrat, O. Christiansen, and B. Kirtman, J. Chem. Phys. **127**, 084118 (2007).
[30]N. F. Zobov, O. L. Polyansky, C. R. Le Sueur, and J. Tennyson, Chem. Phys. Lett. **260**, 381 (1996).
[31]G. Maroulis, Chem. Phys. Lett. **195**, 85 (1992).
[32]J. M. Luis, H. Reis, M. Papdopoulos, and B. Kirtman, J. Chem. Phys. **131**, 034116 (2009).